Anal Bioanal Chem (2015) 407:8067–8077
DOI 10.1007/s00216-015-8979-5

RESEARCH PAPER

# Optical investigation of osteoarthritic human cartilage (ICRS grade) by confocal Raman spectroscopy: a pilot study

**Rajesh Kumar[1] · Kirsten M. Grønhaug[2] · Nils K. Afseth[3] · Vidar Isaksen[4] · Catharina de Lange Davies[1] · Jon O. Drogset[5] · Magnus B. Lilledahl[1]**

Received: 24 May 2015 / Revised: 12 August 2015 / Accepted: 13 August 2015 / Published online: 29 August 2015


**Abstract** Biomolecular changes in the cartilage matrix during the early stage of osteoarthritis may be detected by Raman spectroscopy. The objective of this investigation was to determine vibrational spectral differences among different grades (grades I, II, and III) of osteoarthritis in human osteoarthritic cartilage, which was classified according to the International Cartilage Repair Society (ICRS) grading system. Degenerative articular cartilage samples were collected during total joint replacement surgery and were classified according to the ICRS grading system for osteoarthritis. Twelve cartilage sections (4 sections of each ICRS grades I, II, and III) were selected for Raman spectroscopic analysis. Safranin-O/Fast green was used for histological staining and assignment of the Osteoarthritis Research Society International (OARSI) grade. Multivariate principal component analysis (PCA) was used for data analysis. Spectral analysis indicates that the content of disordered coil collagen increases significantly during the early progression of osteoarthritis. However, the increase was not statistically significant during later stages of the disease. A decrease in the content of proteoglycan was observed only during advanced stages of osteoarthritis. Our investigation shows that Raman spectroscopy can classify the different stage of osteoarthritic cartilage and can provide details on biochemical changes. This proof-of-concept study encourages further investigation of fresh cartilage on a larger population using fiber-based miniaturized Raman probe for the development of in vivo Raman arthroscopy as a potential diagnostic tool for osteoarthritis.

**Keywords** Raman spectroscopy · Osteoarthritis · Cartilage · Collagen · Biomedical optical analysis

**Electronic supplementary material** The online version of this article (doi:10.1007/s00216-015-8979-5) contains supplementary material, which is available to authorized users.

✉ Rajesh Kumar
101rajesh@gmail.com

[1] Department of Physics, Norwegian University of Science and Technology (NTNU), 7491 Trondheim, Norway

[2] Orthopaedic Department, Levanger Hospital, Kirkegata 2, 7600 Levanger, Norway

[3] Nofima, Postbox 210, 1431 Ås, Norway

[4] Department of Medical Biology, The Arctic University of Norway (UiT), 9037 Tromsø, Norway

[5] Department of Orthopaedic Surgery, Trondheim University Hospital, 7491 Trondheim, Norway

## Introduction

Osteoarthritis is a musculoskeletal disorder whose origin is not exactly clear. It is believed that the disease affects the quality of articular cartilage, both collagen and other extracellular matrix (ECM) components, as well as the associated underlying bone. Imaging and biochemical analysis of musculoskeletal tissues are essential tools for diagnostics and therapeutic assessment in orthopedics. Although the use of the Kellgren-Lawrence (K/L) score is a widely accepted method [1], several studies have demonstrated the complexity involved in early-stage diagnosis of osteoarthritis [2–6].

Currently used clinical imaging modalities (e.g., CT, MRI) provide unique and often complementary information to the rheumatologist. However, these modalities fail to provide crucial information about the biochemical composition of the ECM at the molecular level. Even though biochemical changes can be correlated with macroscopic features in musculoskeletal disorders [7], a technique that can detect changes at

the molecular level during the early stages of disease is still awaited.

Over the past decade, light-based vibrational spectroscopic techniques such as Fourier transform infrared spectroscopy (FTIR) and Raman spectroscopy have been employed to study several components of the ECM in musculoskeletal tissues [8–11]. These techniques can be used to obtain information about the biochemical composition and the chemical environment of relevant molecules. However, a major limitation of FTIR is extensive tissue preparation (including dehydration). Raman spectroscopy, on the other hand, provides similar chemical information, potentially in vivo, without any external labeling or preparation of the tissue [12, 13]. In Raman spectra, a series of peaks correspond to different molecular bonds, which may be assigned to specific molecules. The intensity of these peaks is proportional to the content of the corresponding molecular components. Hence, these spectra serve as biochemical fingerprints of the tissue and can be further analyzed to provide physiochemical information. Furthermore, the technique can be used for imaging with submicron spatial resolution [14].

Most studies of osteoarthritis using Raman spectroscopy are focused on the analysis of bone [11, 15–20]. Compared to cartilage, some tissue constituents of bones are relatively strong Raman scatterers and hence provide a strong Raman signal for biochemical analysis. However, the underlying bone is exposed only at an advanced stage of osteoarthritis (i.e., ICRS grade IV), so to detect early-stage osteoarthritis in vivo, it is necessary to perform Raman analysis on the articular cartilage rather than on the bone.

Over the past few years, several groups have used Raman spectroscopy to analyze the properties of articular cartilage and associated disease [21]. However, most studies have focused on the assignment and the structure of the Raman bands [22, 23] in the articular cartilage. By investigating osteoarthritic femoral head sections, Kontoyannis et al. assigned a few Raman bands to illustrate the difference between articular cartilage and subchondral bone [24]. Lim et al. and Pudlas et al. demonstrated the potential of Raman spectroscopy for the detection of proteoglycan changes in cartilage using an animal model [25, 26]. In a view of clinical relevancy, it is necessary to investigate human cartilage, especially primary osteoarthritis, the most common variant. An analysis of differences in human articular cartilage by Raman spectroscopy during progression of osteoarthritis (described by ICRS grade, Electronic Supplementary Material Table S2, [27–29]) is still missing. In case of osteoarthritis, changes at the molecular level in bone and synovial fluid were shown to occur before the appearance of any macroscopic changes in radiography [7, 17, 23, 30, 31]. Investigations of articular cartilage at the molecular level could therefore be important in understanding the underlying mechanism of osteoarthritis. Raman spectroscopy for cell and tissue analysis generally uses visible/near-infrared light. Therefore, the optics involved in Raman spectroscopy are compatible with modern clinical arthroscopes. Hence, with the advancement of technology and development of a miniaturize Raman probe, the technique of Raman spectroscopy can be applied in a clinical setting. Our proof-of-concept study demonstrates the capability of Raman spectroscopy as a potential tool for grading the osteoarthritic cartilage from the formalin-fixed tissue samples. The aim of our pilot study was to demonstrate the feasibility of Raman spectroscopy for the classification and a relative biochemical analysis in different stages of human osteoarthritic cartilage. In this article, we report a Raman spectroscopic investigation in human osteoarthritic cartilage for (i) the classification of different stages of osteoarthritic cartilage, (ii) a relative assessment of change in secondary structure of proteins during progression of osteoarthritis, (iii) a relative assessment of proteoglycan content, and (iv) a quantitative relationship between two standard clinical grading systems (ICRS vs. OARSI) of osteoarthritis.

## Materials and methods

### Confocal Raman microspectrometer

Raman spectra were acquired using a commercial upright confocal Raman microscope (LabRam HR800 HORIBA Jobin Yvon). Briefly, the Raman system was equipped with a 632.10 nm laser used for excitation and was coupled confocally to a spectrograph with a focal length of 800 mm equipped with a grating of 600 g/mm. The laser light was tightly focused using an Olympus ×60, 1.2 NA, water-immersion objective. Scattered Raman photons from the sample were collected in the backscattered geometry by the same microscope objective, passed through a slit-width of 100 μm, and collected by the spectrometer, resulting in a spectral resolution of ~2 $cm^{-1}$. The spectrometer was equipped with an air-cooled deep depletion CCD array detector (1024×256 pixels). The laser power at the tissue surface was 8 mW. The spectra were calibrated to a standard silicon reference peak at 520.7 $cm^{-1}$.

### Sample preparation and classification

The use of human tissues in this study was approved by the Regional Committee for Medical Research Ethics (2013/265 REK, Norway), and patient's informed consent was obtained. Articular cartilage samples were obtained from osteoarthritic patients undergoing total knee replacement surgery. It was confirmed that no patient had suffered any injury and had undergone other prior surgery. Raman spectra were acquired from the 12 cartilage sections that were collected from the knee of 3 patients. Four cartilage sections of International

Cartilage Repair Society (ICRS) grade I, four cartilage sections of ICRS grade II, and four cartilage sections of ICRS grade III were obtained. The contribution of each patient in collection of cartilage sections is shown in the Electronic Supplementary Material Table S1. All samples were harvested from the femoral condyle of the knee during total knee replacement surgery (arthroplasty). The spectra of bone can easily be differentiated from those of cartilage; hence, ICRS grade IV (exposed bone) was not included in the study. Additionally, a total of 21 samples (including the tissues used for Raman analysis) were collected for histological evaluation. The grading of osteoarthritis was based on the standard ICRS classification shown in the Electronic Supplementary Material Table S2. The assignment of ICRS grades were performed by two experienced orthopedic surgeons, who were blinded to the classification of each other. Only samples assigned a similar ICRS grade by both orthopedic surgeons were included in this study. A representative image of cartilage of ICRS grades I, II, and III obtained from a patient is shown in the Electronic Supplementary Material Fig. S2.

The cartilage samples were dissected with a surgical scalpel, perpendicular to the articular surface (from the superficial layer to the subchondral bone) in a cubical shape whose sides were approximately 3–4 mm, fixed in formalin, and stored at 4 °C. For articular cartilage, formalin fixation is recommended by the Histology Endpoint Committee of the ICRS [32]. Previously, it was found that formalin fixation has little effect on vibrational spectra of matrix proteins [33], and it does not cause significant alterations in the Raman spectra of tissues [34–36, 22]. In general, the major change that was observed due to formalin fixation was overall decrease in intensity of spectral peaks [37]. We performed a relative analysis (based on the ratio of peak intensity) in osteoarthritic samples. Therefore, overall reduction in spectral intensity is not a critical issue in our investigation. Moreover, as recommended by Huang et al. [37], to minimize any fixation artifacts, the cartilage sections were thoroughly washed in phosphate-buffered saline (PBS) before Raman measurements. Samples were placed on a small petri dish in such a way that the subchondral bone was at the bottom of the petri dish and the superficial layer of the cartilage was facing the microscope objective. The petri dish was filled with PBS in order to prevent dehydration of the cartilage during measurement. The sample was stable on the surface of the petri dish throughout the measurement. The uppermost exposed articular surface was kept in focus during data acquisition. The data were collected, at randomly chosen points on the articular surface of the cartilage. During random selection of the points, there was sometimes slight change in focus observed due to inherent curvature of the articular surface. However, the observed change in focus was very little. In order to compensate any change in focus and acquire the high-quality spectra, re-focusing was performed, whenever required. The associated background signal (from PBS) was collected separately at each different focus for data pre-processing.

## Spectral acquisition and data analysis

The pre-processing of spectra and data analysis was performed in Matlab (The MathWorks, 2014). The intensities of vertical pixels of CCD were binned to generate the Raman spectra [38]. Subsequently, the unavoidable spurious spikes in the Raman spectra due to cosmic rays were removed by applying the median filter to the raw data set [39]. Because the raw spectra obtained from each tissue sample were composed of Raman signals, autofluorescence and several noise components, the mean of the corresponding background spectra that was acquired from the surrounding medium (PBS) was subtracted from the raw data to remove the interfering signals. In order to enhance the comparability of spectra [40–44], each spectrum was then smoothed (Savitzky-Golay filter, third order, 9 point), and peak normalization (1004 $cm^{-1}$) was performed (Electronic Supplementary Material Fig. S3).

Biological tissues are, in general, chemically heterogeneous at the micrometer level, and therefore data acquired from a small focal volume [45, 46] may account for a local variations at the micrometer level. Therefore, a single measurement may not be representative of the chemical composition of the sample as a whole. Therefore, spectra were collected from 27 different locations (as large as practically feasible) (for details please see Electronic Supplementary Material Fig. S1). Furthermore, to find the spectra of each ICRS grade that represent the composition of the bulk sample as a whole, and minimize the biochemical heterogeneity at submicron level [47] including any influence of instrument (and/or ambient) response, 108 spectra were spectrally averaged (see Electronic Supplementary Material Fig. S1) over the number of cartilage sections of same ICRS grade ($n$=4), for every spectral wavelength position. Therefore, finally 27 spectra ($n$=27) of each ICRS grade (I, II, and III) were obtained and subjected to further statistical analysis. Spectral acquisitions were collected over the region 800–1725 $cm^{-1}$, the fingerprint region of cartilage tissue. The acquisition time for each Raman spectrum was 20 s. To compare the spectra obtained from different ICRS osteoarthritic grades of cartilage, multivariate analysis [48–52] was carried out. Principal component analysis (PCA) was selected to compare data in an unsupervised manner to rule out any subjective bias. For the assessment of diagnostic capability (specificity and sensitivity) and prediction efficiency of Raman spectroscopy for the classification of the tissue, the assignment of ICRS grade was chosen as gold standard. ICRS grading system was chosen as this is commonly used in arthroscopic investigations by orthopedic surgeons.

### Histological staining

Aggrecan, the core protein of proteoglycans in cartilage, is bound to a large number of glucosaminoglycans (GAGs). Safranin-O is a basic dye that binds to the acidic GAGs and appears orange in color [53]. Safranin-O/Fast Green staining is preferred over standard H&E staining because the former provides qualitative information about the proteoglycan content.

After Raman spectroscopy measurement, each tissue was stored in 10 % neutral-buffered formalin (NBF), dehydrated, and embedded in paraffin. The tissue was sectioned perpendicular to the articular surface and mounted on glass slides. The sections were deparaffinized in Tissue-Clear® (Sakura) and rehydrated using decreasing ratios of ethanol to water. Slides were stained with Weigert's iron hematoxylin (Sigma-Aldrich®) and then rinsed in water before incubation in Fast Green, differentiated in acetic acid, and stained with Safranin-O (Sigma-Aldrich®) with a Sakura Tissue-Tek Prisma automatic stainer. Dehydration of the slides was performed using 95 % and absolute ethanol. Tissue-Clear was used, before mounting the section by Sakura Tissue-Tec Glas automatic coverslipper. Based on morphological and Safranin-O evaluation, each tissue sample was assigned to a specific Osteoarthritis Research Society International (OARSI) grade (Electronic Supplementary Material Table S3) [54].

### Statistical analysis

The relative change in protein (disordered/ordered) coil content and proteoglycan content in osteoarthritic articular cartilage were investigated by the analysis of region of interest (ROI)-1 and ROI-2 respectively (Fig. 1). Multiple-group statistical comparisons among different ICRS osteoarthritic grades were assessed by nonparametric Kruskal-Wallis ANOVA test using Matlab (The MathWorks, 2014). In total 108 Raman spectra, 27 representative spectra obtained from each ICRS grade (i.e., group) of osteoarthritic cartilage were used for Kruskal-Wallis test. The assumptions (i.e., independent measurements, non-normal distribution, and similar variability) of Kruskal-Wallis test were verified. Box plots display median values and interquartile ranges. In all multiple-group pairwise comparisons, a $p$ value of less than 0.05 was considered indicative of statistical significance. The degree of association between OARSI and ICRS grades was expressed by the coefficient of determination $R^2$, and result was presented as a mean value±standard error using the software IBM SPSS 21.0 (SPSS Inc., Chicago, Illinois).

## Results and discussion

A comparison between the mean (of $n$=108 spectra) Raman spectra of ICRS grades I, II, and III with standard error is shown in Fig. 1. Distinguishable Raman bands corresponding to the different grades of osteoarthritis were observed. These bands are associated with different vibrational modes of biochemical components present inside the cartilage matrix [22, 25]. Figure 1 shows the spectra obtained from ICRS grades I, II, III, and IV tissues. As mentioned in the "Materials and methods" section, the spectra of bone (grade IV) can be easily distinguished from the spectra of cartilage (grades I, II, and III) because of the presence of minerals (e.g., carbonate peak at 1070 $cm^{-1}$ and phosphate peak at 960 $cm^{-1}$) inside bone. Hence, in view of finding spectral differences among degraded cartilage, only cartilage of grades I, II, and III and without exposed bone (grade IV), which appears in the advanced stage of osteoarthritis, was

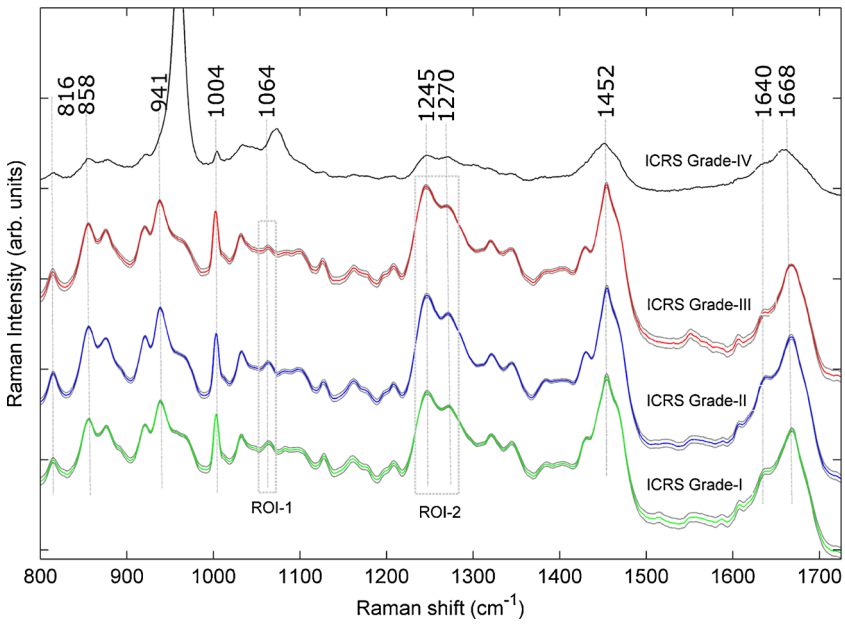


**Fig. 1** Mean ($n$=108 spectra) normalized Raman spectra obtained from ICRS grades I, II, III, and IV tissues. Spectra are offset for clarity. The *solid lines* indicate the average spectra while the *shaded lines* represent the standard error. Region of interest (ROI)-1 shows the peak at 1064 $cm^{-1}$, whereas ROI-2 shows the peaks at 1245 and 1270 $cm^{-1}$. Separate statistical test was performed for ROIs. The band at 960 $cm^{-1}$ in the spectra from grade IV (*black color*) is out of scale and hence truncated

analyzed. The loss of proteoglycans in articular cartilage is a hallmark in the osteoarthritic process. In order to find the changes in content of proteoglycan in human cartilage, the Raman peak at 1064 $cm^{-1}$ (ROI-1) was chosen because it is the representative peak of proteoglycan [22, 25, 26]. Change in content of defective collagen was shown in earlier studies [55, 56]. To find such changes in ICRS grade of osteoarthritic human cartilage, the doublet Raman peak at 1245 and 1270 $cm^{-1}$ (ROI-2) were chosen [55–58]. The analyses of two region of interests (ROIs), as shown in Fig. 1, were performed separately and are described in the following sections.

### Principal component analysis

To determine the classification ability (similarities or differences among spectra) of Raman spectroscopy, 81 Raman spectra (27 spectra of each ICRS grades I, II, and III) obtained from osteoarthritic cartilage were subjected to PCA. PCA was performed on the raw data matrix by using Matlab (The MathWorks, 2014). Principal components were obtained by the eigen-decomposition of covariance matrix which is created from the data set [59]. PCA reduces the dimensionality of the data set by finding an alternative set of co-ordinates [60]. The general form of PCA model is as follows:

$$X = YZ^{Y} + Q \tag{1}$$

Where $X$ matrix is decomposed by PCA into two smaller matrices that are called scores ($Y$) and loadings ($Z$). PCA is performed by the transformation of a large number of correlated variable (i.e., Raman shifts) into smaller number of uncorrelated variables called principal components. Numerically, it is represented as

$$\sum_{j=1}^{J} y_{ja}\, y_{jb} = 0 \tag{2}$$

where $y_a$ and $y_b$ are the $a^{th}$ and $b^{th}$ column of $Y$ matrix, respectively and

$$\sum_{j=1}^{J} z_{ja}\, z_{jb} = 0 \tag{3}$$

where $z_a$ and $z_b$ are the $a^{th}$ and $b^{th}$ rows of $Z$ matrix, respectively.

The first principal components (PC1) account for the maximum variability of the dataset. Each succeeding component (PC2, PC3, etc.) accounts for progressively smaller amounts of variance. The results of the PCA analysis are shown in Figs. 2 and 3. Figure 2 shows the data plotted against the three main PCs. Each Raman spectrum is represented by a single point in the cluster. The color of the data points represents a specific ICRS grade. The data were observed to cluster into separated groups. Figure 3a–c shows the loading vectors associated with PC-3, PC-2, and PC-1, respectively.

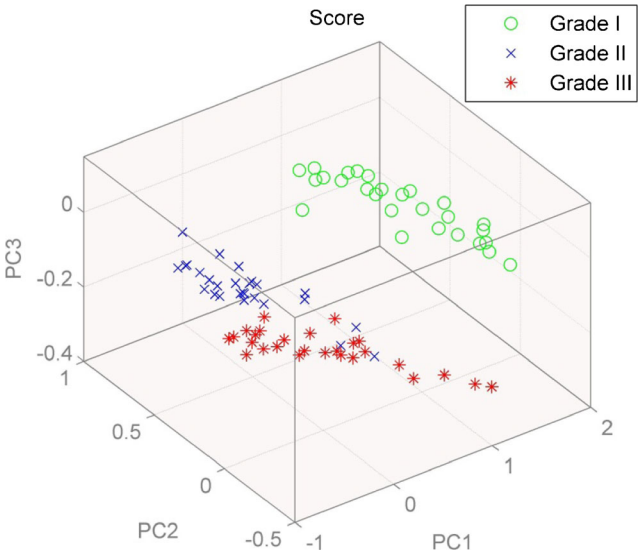


**Fig. 2** Multivariate analysis-based PCA algorithm classifies different ICRS grades of osteoarthritis into separate clusters (grade I: *green circle*, grade II: *blue cross*, and grade III: *red asterisk*)

As shown in Fig. 2, the spectra associated with different grades of osteoarthritis appear as distinct clusters when plotted against the three main PCs. In order to discriminate different clusters quantitatively, prediction accuracy was tested by performing leave-one-out cross-validation [60, 61] using Mahalanobis distance as a discriminator. Accordingly, a confusion matrix was constructed which summarizes the correct and incorrect classification of the spectra (Table 1). Each row of the confusion matrix provides the predicted classification for a specific ICRS grade. The diagonal terms of the confusion matrix provide the number of correct predictive classification for the three different ICRS grade. Hence, the average of these diagonal values provides the predictive efficiency of the predictive classification. By the use of confusion matrix, discrimination capability of PCA was calculated in terms of specificity and sensitivity. The specificity for ICRS grades I, II, and III was 87.0, 90.1, and 100 % respectively, while sensitivity was 81.4, 85.1, and 88.8 % respectively. The overall predictive efficiency was approximately 85 %. The high specificity, sensitivity, and efficiency obtained from multivariate analysis on Raman spectra of different ICRS grade demonstrate the potential of Raman spectroscopy as a label free, rapid, and accurate optical tool for classification of the stage of osteoarthritis based on the vibrational spectra of articular cartilage.

To determine the biochemical composition, which is responsible for the separation of the data into three distinct clusters, we plotted the loading spectra (Fig. 3) of the principal components. PC-1, PC-2, and PC-3 explain 84.23, 12.36, and 1.91 % of the total variance in the data set, respectively. Combined, these three PCs explain 98.50 % of the total variation in the data set. Other PCs account for various sources of

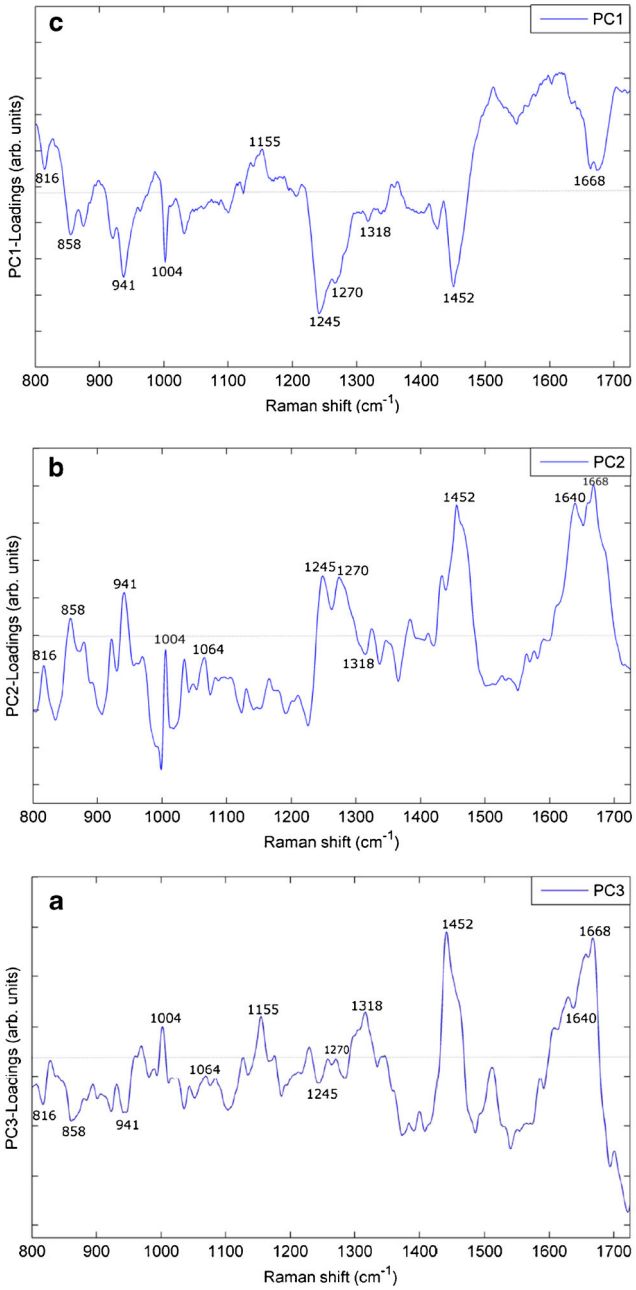


**Fig. 3** Loading plot associated with **a** PC 1, **b** PC 2, and **c** PC 3, which are mainly responsible for the discrimination between samples of different grades of osteoarthritis

noise in the data set. The loading plots associated with PC-1, PC-2, and PC-3 show the spectral features associated with the cartilage matrix at 1668, 1640, 1452, 1270, 1245, 1064, 1004, 941, 858, and 816 $cm^{-1}$. Although it is not straightforward to assign the biochemical Raman peaks associated with each spectral feature observed in the PC-loading plot, we tentatively assigned the corresponding molecular vibrations listed in Table 2. Two spectral peaks (1128 and 1321 $cm^{-1}$) remain unassigned. The origin of these bands is not yet clear and needs further investigation.

**Table 1** Confusion matrix shows the classification for each ICRS grade of osteoarthritic cartilage

| Sample | Predicted classification | | |
|---|---|---|---|
| | Grade I | Grade II | Grade III |
| Grade I (27) | 22 | 5 | 0 |
| Grade II (27) | 4 | 23 | 0 |
| Grade III (27) | 3 | 0 | 24 |

## Analysis of relative amide content

Raman spectroscopy is able to provide information about protein structure. Subtle molecular changes often cause detectable vibrational changes that can be detected by Raman analysis [55]. Thus, Raman spectroscopy may be useful in differentiating between normal and pathological cartilage. The doublet Raman peaks at 1245 and 1270 $cm^{-1}$ were shown by ROI-2 in Fig. 1. The intensity ratio of two peaks ($I_{1245}/I_{1270}$) provides information about the relative content of random vs. ordered coil in the protein structure [55–58].

Figure 4 shows that the median value of the intensity ratio ($I_{1245}/I_{1270}$) increases with the ICRS grade. To determine whether this ratio varies significantly among different ICRS grades of osteoarthritic cartilage, we performed a nonparametric Kruskal-Wallis ANOVA test; the results are summarized in Fig. 4. Multiple-group pairwise analysis revealed that the median difference was statistically significant ($p<0.0001$) between grades I and II and between grades I and III but not between grades II and III.

As Fig. 4 indicates that the median value of the intensity ratio ($I_{1245}/I_{1270}$) increases with the ICRS grade, which means that the ratio of the random to ordered protein coil content changes with the progression of the cartilage disorder. This finding indicates an increase in the content of defective collagen [55] and illustrates the ability of Raman spectroscopy to detect minute modifications in the cartilage structure.

**Table 2** Wavenumber ($cm^{-1}$) and respective vibrational assignment in human articular cartilage [22, 24–26, 57, 58]

| Wavenumber ($cm^{-1}$) | Assignment |
|---|---|
| 1668 | C-O stretch; amide I- α helix |
| 1640 | Amide I- collagen secondary str. |
| 1452 | $CH_2/CH_3$ scissoring; collagen and other protein |
| 1270 | ($NH_2$) bending; amide III-ordered coil |
| 1245 | ($NH_2$) bending; amide III-disordered coil |
| 1064 | $SO_3^-$ stretching; glycoaminoglycan |
| 1004 | Phenylalanine ring breathing |
| 941 | C-C stretching; collagen |
| 858 | C-C stretching; proline |
| 816 | C-C stretching; protein backbone |

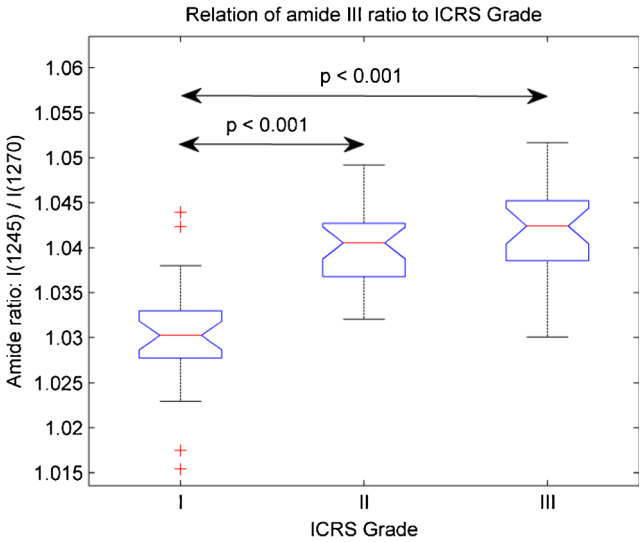


**Fig. 4** Comparison ($n$=27 spectra) of relative amide III content in tissues of different grades of osteoarthritis. The dependence of the ratio of random vs. ordered protein coil content is shown as a function of ICRS grade. The symbol "*plus sign*" represents outliers in the data set

However, it should also be noted that although the median value increases from the grade II group to the grade III group, the increment is not statistically significant. This result suggests that during the progression of osteoarthritis from grade I to grade II, the increase in the disordered coil (defective collagen) content is quite high, whereas during the progression of the disease from grade II to grade III, the increase is not statistically significant. This trend may arise because during the early progression of the disease, biochemical changes play a significant role, whereas later, at more advanced stages of osteoarthritis, due to the increase in the frictional coefficient between the contact cartilage surfaces, mechanical effects become more dominant than biochemical effects, and the load-bearing surfaces start to wear out. Overall, this analysis indicates that the disordered coil content inside the cartilage matrix increases significantly during the early progression of osteoarthritis (between grades I and II). However, such increment was not statistically significant during higher stage progression of osteoarthritis (between grades I and II). This observation is in agreement with that made in a previous study [56]. The relative content of the secondary structure of collagen may play an important role as a biomarker in the early diagnosis of the disease.

## Analysis of proteoglycan content

Proteoglycan is a major component of the ECM in cartilage. The protein accounts for approximately 40 % of the dry weight of cartilage and is responsible for providing the osmotic resistance necessary for cartilage to resist compressive loads [62]. Based on previous reports, we chose the peak at 1064 $cm^{-1}$ as the most representative peak of proteoglycan [22, 25, 26]. The peak at 1064 $cm^{-1}$ is illustrated by ROI-1 in Fig. 1. The intensity ratio of the two peaks ($I_{1064}/I_{1004}$) provides an indication of proteoglycan content in ECM of cartilage because the peak at 1004 $cm^{-1}$ is generally assumed to be the most stable Raman peak against any changes in the local environment of tissue [63]. To determine the statistical significance of the differences in the proteoglycan content among the different ICRS grades of osteoarthritic cartilage, we performed a nonparametric Kruskal-Wallis ANOVA; the results are summarized in the Fig. 5. It shows two results. First, there is a decrease in the median value associated with proteoglycan content during the progression of osteoarthritis. Second, a multiple-group pairwise test reveals that the difference between the grades I and II groups is not statistically significant, whereas the differences between the grades I and III groups and the grades II and III groups are statistically significant ($p$<0.0001 and $p$<0.001, respectively).

It has been reported that to compensate for the loss of proteoglycan during the progression of joint degenerative disease, the synthesis rate of proteoglycan increases during the early stages (low grade) of osteoarthritis, whereas it decreases in advanced stages (high grade) of disease [64–66]. As indicated by the results shown in Fig. 5, although there is a decrease in the median value of the proteoglycan content (represented by the value of $I_{1064}/I_{1004}$) during the progression of osteoarthritis, the difference between the grades I and II groups is not statistically significant, perhaps because the rate of proteoglycan synthesis is relatively high during the early stages of disease, and hence, the net loss in the proteoglycan content may not be sufficiently high to be statistically significant between grades I and II.

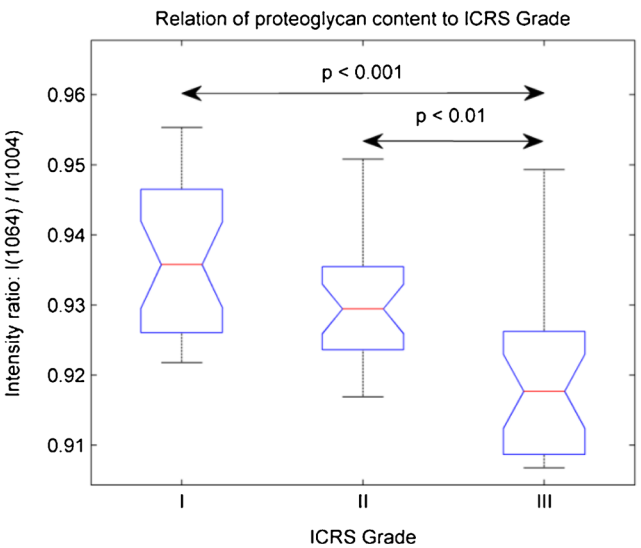


**Fig. 5** A relative comparison ($n$=27 spectra) of proteoglycan contents in tissues of different grades of osteoarthritis. The dependence of the proteoglycan content inside the cartilage matrix is shown as a function of ICRS grade of osteoarthritis

Furthermore, due to the decrease in the synthesis rate of proteoglycan during the advanced stages of the disease, the net loss of proteoglycan becomes quite high between grades II and III and distinctly so between grades I and III. Hence, the differences between grade II and III and between grades I and III are statistically significant. In conclusion, by Raman spectroscopic analysis, we have shown that the net loss of proteoglycan content was only significant at advanced stages of osteoarthritis. This result is in agreement with previous reports based on metabolic analysis [64–66].

### Histological analysis

A qualitative histological analysis showed higher degradation of cartilage during progression of osteoarthritis (from ICRS grade I to grade III). Representative histological images of ICRS grades I, II, and III are shown in Fig. 6. In sections from ICRS grade I (Fig. 6a), a thin, pale–green/orange layer shows the superficial region of the articular cartilage, which appears smooth with only slight erosions, whereas in sections from grade II (Fig. 6b), the superficial layer has almost disappeared, fibers are relatively more fibrillated, and cracks progress down to the middle zone. Sections from grade III (Fig. 6c) show significant fragmentation, quite thick fibers in the middle zone, and cracks propagating down to the deep region. Sections from grade IV show some remnants of cartilage and otherwise only exposed bone surface. A clear increase in morphological disarrangement was indicated by the histological evaluation with a progressive increase in ICRS grade.

To assess the histological images quantitatively, slides were classified and given a specific grade of osteoarthritis from I to VI based on the OARSI grading system (Electronic Supplementary Material Table S3) [54]. Higher OARSI grades were observed with increasing values of ICRS grade. The mean OARSI grades for ICRS grades I, II, III, and IV were 0.92±0.2, 2.12±0.65, 3.57±0.25, and 5.37±0.62, respectively (Fig. 7). A significant correlation was observed between the OARSI and ICRS grades ($R^2$=0.789, $p$<0.01).

Based on the histological analysis of ICRS grades I, II, and III, we can conclude that in addition to the progressive thinning of the cartilage (consistent with previous reports [67–69]), the morphological disorder of collagen fibers increases with ICRS grade, and hence, the results of qualitative histological evaluation are observed to be in agreement with the ICRS classification (Electronic Supplementary Material Table S2) [27–29] of the specimens. Moreover, quantitatively, a high positive correlation was observed between the results of ICRS assessment (Electronic Supplementary Material Table S2) by orthopedic surgeons and those obtained by OARSI-template-based (Electronic Supplementary Material Table S3) histological evaluation. This high positive correlation indicates that macroscopic evaluation (e.g., during surgery or arthroscopy) may be a suitable method for classifying degraded cartilage.

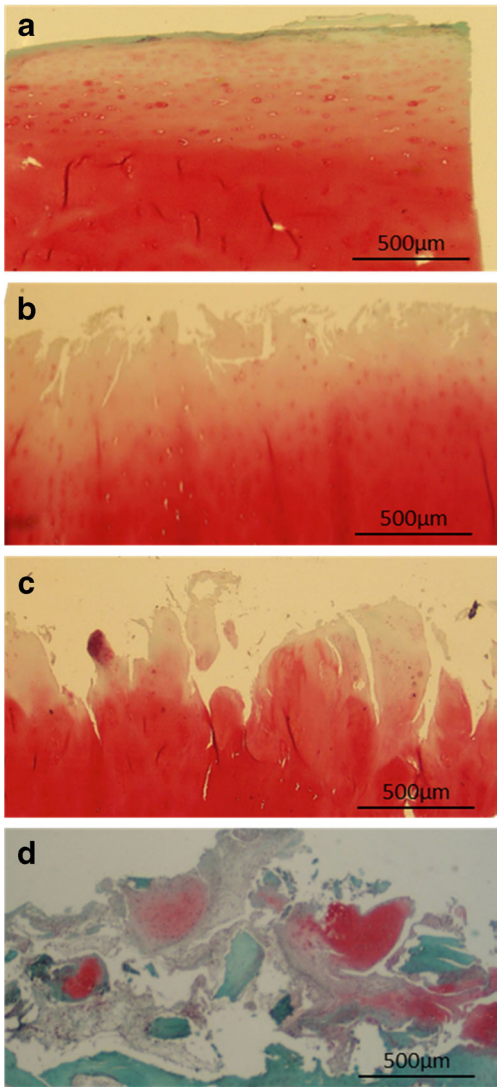


**Fig. 6** Histological image of osteoarthritic cartilage stained by Safranin-O/Fast Green. **a** ICRS grade I, **b** ICRS grade II, **c** ICRS grade III, and **d** ICRS grade IV. Distribution of proteoglycan is illustrated in *orange/red*

## Conclusion

In conclusion, our study show that Raman spectroscopy could be a potential label-free optical tool which, with high specificity and sensitivity, can detect the biomolecular change in human articular cartilage and can classify different stages (i.e., ICRS grades) of osteoarthritis based on spectral properties. We were also able to provide information about the biochemical modification of the cartilage matrix during the progression of osteoarthritis in terms of the relative contents of ordered and disordered protein coils, which may potentially serve as biomarker in the early diagnosis of

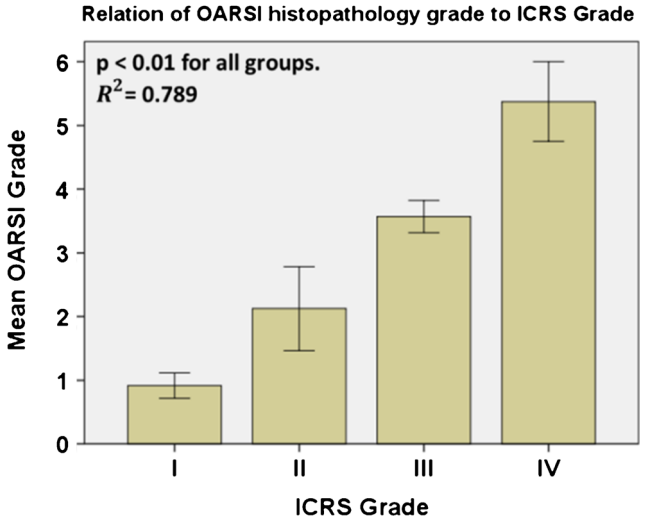


**Fig. 7** Mean OARSI grade as a function of ICRS grade of osteoarthritis ($n$=21 cartilage sections). A high correlation exists between the OARSI histological evaluation and macroscopic ICRS assessment

osteoarthritis. Moreover, by Raman spectroscopic investigation, in human model, we have shown that the decrease in proteoglycan content was clearly observed only in advanced stage of osteoarthritis. Both of the results, change in protein content and proteoglycan content, are found to be consistent with progression of osteoarthritis [56, 64–66].

Due to practical reasons, this investigation was performed in formalin-fixed osteoarthritic cartilage sections and therefore caution is needed in extrapolation of conclusion to, e.g., fresh cartilage. Although, the optimum protocol [22, 34–37] developed to handle the formalin-fixed tissue for Raman spectroscopy was followed, additional studies are essential to allow the accurate comparison with fresh cartilage. Further investigations to determine the effects of various fixatives (e.g., alcohol, formalin, paraformaldehyde) specifically on vibrational spectra of cartilage and a comparison with fresh as well as healthy cartilage are currently under way.

The optics involved in Raman spectroscopy are compatible with modern clinical arthroscopy. Therefore, even though confocal Raman spectroscopy is still limited to a laboratory environment, the applied technique can be extended to in vivo diagnosis with the help of a miniaturized Raman fiber probe integrated within a clinical arthroscope, which is currently under development [70]. This pilot study presents a proof-of-concept investigation in human cartilage; however, to validate the assessment ability of the proposed spectroscopic method, further analysis on large number of patients with controls is necessary. Nevertheless, these results encourage further investigations (e.g., quantitative determination of biochemical compositions) on human osteoarthritic cartilage, which may reveal hidden features associated with progression of the disease. Our ongoing research will focus on revealing other biochemical information present in Raman spectra, which may enhance the proposed method's ability to discern degraded cartilage even at early stage of manifestation.

**Acknowledgment** We are pleased to acknowledge Kristin G. Sæterbø, Astrid Bjørkøy, and Ulrike Böcker (Nofima) for their assistance in the laboratory. The histological analysis was performed at the Cellular and Molecular Imaging Core Facility (CMIC), Norwegian University of Science and Technology (NTNU). The partial funding to carry out this study was received from the joint committee of Helse Midt-Norge (HMN)-NTNU, Norway.

**Conflict of interest** The authors declare that they have no conflict of interest.

## References

1. Kellgren JH, Lawrence JS (1957) Radiological assessment of osteo-arthrosis. Ann Rheum Dis 16:494–502
2. Kornaat PR, Bloem JL, Ceulemans RY, Riyazi N, Rosendaal FR, Nelissen RG, Carter WO, Hellio Le Graverand MP, Kloppenburg M (2006) Osteoarthritis of the knee: association between clinical features and MR imaging findings. Radiology 239:811–817
3. Li X, Benjamin Ma C, Link TM, Castillo DD, Blumenkrantz G, Lozano J, Carballido-Gamio J, Ries M, Majumdar S (2007) In vivo T(1rho) and T(2) mapping of articular cartilage in osteoarthritis of the knee using 3 T MRI. Osteoarthritis Cartil / OARS, Osteoarthr Res Soc 15:789–797
4. Raynauld JP, Martel-Pelletier J, Berthiaume MJ, Labonte F, Beaudoin G, de Guise JA, Bloch DA, Choquette D, Haraoui B, Altman RD, Hochberg MC, Meyer JM, Cline GA, Pelletier JP (2004) Quantitative magnetic resonance imaging evaluation of knee osteoarthritis progression over two years and correlation with clinical symptoms and radiologic changes. Arthritis Rheum 50: 476–487
5. Bruyere O, Genant H, Kothari M, Zaim S, White D, Peterfy C, Burlet N, Richy F, Ethgen D, Montague T, Dabrowski C, Reginster JY (2007) Longitudinal study of magnetic resonance imaging and standard X-rays to assess disease progression in osteoarthritis. Osteoarthritis Cartil / OARS, Osteoarthr Res Soc 15:98–103
6. Cicuttini F, Hankin J, Jones G, Wluka A (2005) Comparison of conventional standing knee radiographs and magnetic resonance imaging in assessing progression of tibiofemoral joint osteoarthritis. Osteoarthritis Cartil / OARS, Osteoarthr Res Soc 13:722–727
7. Morris MD, Roessler BJ (2006) Future spectroscopic diagnostics in osteoarthritis. Fut Rheumatol 1:383–386
8. Bi X, Yang X, Bostrom MP, Camacho NP (2006) Fourier transform infrared imaging spectroscopy investigations in the pathogenesis and repair of cartilage. Biochim Biophys Acta 1758(7):934–941
9. Boskey A, Pleshko Camacho N (2007) FT-IR imaging of native and tissue-engineered bone and cartilage. Biomaterials 28:2465–2478
10. West PA, Bostrom MP, Torzilli PA, Camacho NP (2004) Fourier transform infrared spectral analysis of degenerative cartilage: an infrared fiber optic probe and imaging study. Appl Spectrosc 58: 376–381
11. Dehring KA, Crane NJ, Smukler AR, McHugh JB, Roessler BJ, Morris MD (2006) Identifying chemical changes in subchondral bone taken from murine knee joints using Raman spectroscopy. Appl Spectrosc 60:1134–1141
12. Argyri AA, Jarvis RM, Wedge D, Xu Y, Panagou EZ, Goodacre R, Nychas G-JE (2013) A comparison of Raman and FT-IR spectroscopy for the prediction of meat spoilage. Food Control 29:461–470

13. Kumar R, Singh G, Grønhaug K, Afseth N, de Lange DC, Drogset J, Lilledahl M (2015) single cell confocal Raman spectroscopy of human osteoarthritic chondrocytes: a preliminary study. Int J Mol Sci 16:9341–9353
14. Nyman JS, Makowski AJ, Patil CA, Masui TP, O'Quinn EC, Bi X, Guelcher SA, Nicollela DP, Mahadevan-Jansen A (2011) Measuring differences in compositional properties of bone tissue by confocal Raman spectroscopy. Calcif Tissue Int 89:111–122
15. Kerns JG, Gikas PD, Buckley K, Birch HL, McCarthy ID, Miles J, Briggs TWR, Parker AW, Matousek P, Goodship AE (2013) Raman spectroscopy reveals evidence for early bone changes in osteoarthrits. Bone Joint J Orthop Proc Suppl 95-B:45
16. Khan AF, Awais M, Khan AS, Tabassum S, Chaudhry AA, Rehman IU (2013) Raman spectroscopy of natural bone and synthetic apatites. Appl Spectrosc Rev 48:329–355
17. Carden A, Morris MD (2000) Application of vibrational spectroscopy to the study of mineralized tissues (review). J Biomed Opt 5: 259–268
18. Buchwald T, Niciejewski K, Kozielski M, Szybowicz M, Siatkowski M, Krauss H (2012) Identifying compositional and structural changes in spongy and subchondral bone from the hip joints of patients with osteoarthritis using Raman spectroscopy. J Biomed Opt 17:017007
19. Bohic S, Rey C, Legrand A, Sfihi H, Rohanizadeh R, Martel C, Barbier A, Daculsi G (2000) Characterization of the trabecular rat bone mineral: effect of ovariectomy and bisphosphonate treatment. Bone 26:341–348
20. Notingher I, Jell G, Notingher P, Bisson I, Polak J, Hench L (2005) Raman spectroscopy: potential tool for in situ characterization of bone cell differentiation. Bioceramics 17:545–548
21. Boskey AL, Garip S (2012) Diagnosis of bone and cartilage diseases. In: Severcan F, Haris PI (eds) Vibrational Spectroscopy in Diagnosis and Screening, chap. 11. IOS Press: pp 272–303
22. Bonifacio A, Beleites C, Vittur F, Marsich E, Semeraro S, Paoletti S, Sergo V (2010) Chemical imaging of articular cartilage sections with Raman mapping, employing uni- and multi-variate methods for data analysis. Analyst 135:3193–3204
23. Karen AE (2009) R aman spectroscopy detection of molecular changes associated with osteoarthritis. PhD Thesis, University of Michigan
24. Kontoyannis C, Vardaki M, Megas P, Panteliou S, Orkoula M, Papachristou D (2011) Raman spectroscopy of articular cartilage and subchondral bone on osteoarthritic human femoral heads. School of Pharmacy (Publ IP Conference), University of Patras
25. Lim NS, Hamed Z, Yeow CH, Chan C, Huang Z (2011) Early detection of biomolecular changes in disrupted porcine cartilage using polarized Raman spectroscopy. J Biomed Opt 16(1):017003
26. Pudlas M, Brauchle E, Klein TJ, Hutmacher DW, Schenke-Layland K (2013) Non-invasive identification of proteoglycans and chondrocyte differentiation state by Raman microspectroscopy. J Biophotonics 6:205–211
27. Outerbridge RE (1961) The etiology of chondromalacia patellae. J Bone Joint Surg Br Vol 43-b:752–757
28. Kleemann RU, Krocker D, Cedraro A, Tuischer J, Duda GN (2005) Altered cartilage mechanics and histology in knee osteoarthritis: relation to clinical assessment (ICRS Grade). Osteoarthritis Cartil / OARS, Osteoarthr Res Soc 13:958–963
29. Brittberg M et al., ICRS Cartilage Injury Evaluation Package. Proceedings of 3rd ICRS meeting, Göteborg, Sweden., 2000. Available online: http://www.cartilage.org/_files/contentmanagement/ICRS_evaluation.pdf
30. Hoetker MS, Goetz M (2013) Molecular imaging in endoscopy. U Eur Gastroenterol J 1:84–92
31. Popp J, Schmitt M (2013) The Many facets of Raman Spectroscopy in Biophotonics. In: Optics in the Life Sciences, Waikoloa Beach, Hawaii. OSA Technical Digest (online). Optical Society of America, p MT1C.1
32. Mainil-Varlet P, Aigner T, Brittberg M, Bullough P, Hollander A, Hunziker E, Kandel R, Nehrer S, Pritzker K, Roberts S, Stauffer E (2003) Histological assessment of cartilage repair: a report by the Histology Endpoint Committee of the International Cartilage Repair Society (ICRS). J Bone Joint Surg Am Vol 85-A(Suppl 2): 45–57
33. Severcan F, Haris PI (2012) Vibrational Spectroscopy in Diagnosis and Screening. Advances in Biomedical Spectroscopy, Vol 6. IOS Press
34. Salzer R, Siesler HW (2009) Infrared and Raman Spectroscopic Imaging. eds.,Wiley-VCH, Weinheim, Germany
35. Meade A, Clarke C, Draux F, Sockalingum G, Manfait M, Lyng F, Byrne H (2010) Studies of chemical fixation effects in human cell lines using Raman microspectroscopy. Anal Bioanal Chem 396: 1781–1791
36. Kunstar A (2012) Confocal Raman microspectroscopy: application in cartilage tissue engineering. PhD Thesis., University of Twente, Enschede, The Netherlands
37. Huang Z, McWilliams A, Lam S, English J, McLean DI, Lui H, Zeng H (2003) Effect of formalin fixation on the near-infrared Raman spectroscopy of normal and cancerous human bronchial tissues. Int J Oncol 23:649–655
38. Dubessy J, Rull F, Sharma S (2012) Instrumentation in Raman spectroscopy; elementary theory and practice (in Applications of Raman spectroscopy to earth sciences and cultural heritage). Eur Mineral Union Notes Mineral 12:83–172
39. Esmonde-White FWL, Schulmerich MV, Esmonde-White KA, Morris MD (2009) Automated Raman spectral preprocessing of bone and other musculoskeletal tissues. Proc. SPIE: 716605–716610
40. Savitzky A, Golay MJE (1964) Smoothing and differentiation of data by simplified least squares procedures. Anal Chem 36:1627–1639
41. Barman I, Singh GP, Dasari RR, Feld MS (2009) Turbidity-corrected raman spectroscopy for blood analyte detection. Anal Chem 81:4233–4240
42. Zhao J, Lui H, McLean DI, Zeng H (2007) Automated autofluorescence background subtraction algorithm for biomedical Raman spectroscopy. Appl Spectrosc 61:1225–1232
43. Barman I, Kong CR, Singh GP, Dasari RR (2011) Effect of photobleaching on calibration model development in biological Raman spectroscopy. J Biomed Opt 16:011004
44. Kumar R, Singh GP, Barman I, Dingari NC, Nabi G (2013) A facile and real-time spectroscopic method for biofluid analysis in point-of-care diagnostics. Bioanalysis 5:1853–1861
45. Bugay DE (2001) Characterization of the solid-state: spectroscopic techniques. Adv Drug Deliv Rev 48:43–65
46. McCreery RL (2000) Raman spectroscopy for chemical analysis. Wiley-Interscience, New York
47. Rösch P, Harz M, Schmitt M, Popp J (2005) Raman spectroscopic identification of single yeast cells. J Raman Spectrosc 36:377–379
48. Myakalwar AK, Sreedhar S, Barman I, Dingari NC, Venugopal Rao S, Prem Kiran P, Tewari SP, Manoj Kumar G (2011) Laser-induced breakdown spectroscopy-based investigation and classification of pharmaceutical tablets using multivariate chemometric analysis. Talanta 87:53–59
49. Smith E, Dent G (2005) Modern Raman spectroscopy: a practical approach. Wiley.
50. Stone N, Kendall C, Smith J, Crow P, Barr H (2004) Raman spectroscopy for identification of epithelial cancers. Faraday Discuss 126:141–157, **discussion 169–183**
51. Stone N, Stavroulaki P, Kendall C, Birchall M, Barr H (2000) Raman spectroscopy for early detection of laryngeal malignancy: preliminary results. Laryngoscope 110:1756–1763

52. Barman I, Dingari NC, Singh GP, Kumar R, Lang S, Nabi G (2012) Selective sampling using confocal Raman spectroscopy provides enhanced specificity for urinary bladder cancer diagnosis. Anal Bioanal Chem 404:3091–3099
53. Rosenberg L (1971) Chemical basis for the histological use of safranin O in the study of articular cartilage. J Bone Joint Surg Am Vol 53:69–82
54. Pritzker KP, Gay S, Jimenez SA, Ostergaard K, Pelletier JP, Revell PA, Salter D, van den Berg WB (2006) Osteoarthritis cartilage histopathology: grading and staging. Osteoarthritis Cartil / OARS, Osteoarthr Res Soc 14:13–29
55. Dehring KA, Smukler AR, Roessler BJ, Morris MD (2006) Correlating changes in collagen secondary structure with aging and defective type II collagen by Raman spectroscopy. Appl Spectrosc 60:366–372
56. Takahashi Y, Sugano N, Takao M, Sakai T, Nishii T, Pezzotti G (2014) Raman spectroscopy investigation of load-assisted microstructural alterations in human knee cartilage: preliminary study into diagnostic potential for osteoarthritis. J Mech Behav Biomed Mater 31:77–85
57. Bonifacio A, Sergo V (2010) Effects of sample orientation in Raman microspectroscopy of collagen fibers and their impact on the interpretation of the amide III band. Vib Spectrosc 53:314–317
58. Lednev IK, Karnoup AS, Sparrow MC, Asher SA (1999) Nanosecond UV resonance Raman examination of initial steps in α-helix secondary structure evolution. In: Puppels GJ, Otto C (eds) Greve J. Spectroscopy of Biological Molecules, New Directions. Springer Netherlands, pp 11–12
59. Abdi H (2007) The eigen-decomposition: eigenvalues and eigenvectors. Salkind NJ (Ed.), Encyclopedia of Measurement and Statistics. Sage Publications
60. Mobili P, Londero P, De Antoni G, Gomez-Zavaglia A (2010) Multivariate analysis of Raman spectra applied to microbiology: discrimination of microorganisms at the species level. Revista Mexicana De Fisica 56:378–385
61. Sahu A, Dalal K, Naglot S, Aggarwal P, Murali Krishna C (2013) Serum based diagnosis of asthma using Raman spectroscopy: an early phase pilot study. PLoS One 8
62. Knudson CB, Knudson W (2001) Cartilage proteoglycans. Semin Cell Dev Biol 12(2):69–78
63. Fischer WB, Eysel HH (1992) Polarized Raman spectra and intensities of aromatic amino acids phenylalanine, tyrosine and tryptophan. Spectrochim Acta A: Mol Spectrosc 48(5):725–732
64. Rizkalla G, Reiner A, Bogoch E, Poole AR (1992) Studies of the articular cartilage proteoglycan aggrecan in health and osteoarthritis. Evidence for molecular heterogeneity and extensive molecular changes in disease. J Clin Invest 90(6):2268–2277
65. Thompson RC Jr, Oegema TR Jr (1979) Metabolic activity of articular cartilage in osteoarthritis. An in vitro study. J Bone Joint Surg Am Vol 61(3):407–416
66. Mankin HJ, Dorfman H, Lippiello L, Zarins A (1971) Biochemical and metabolic abnormalities in articular cartilage from osteoarthritic human hips. II. Correlation of morphology with biochemical and metabolic data. J Bone Joint Surg Am Vol 53(3):523–537
67. Radin EL, Rose RM (1986) Role of subchondral bone in the initiation and progression of cartilage damage. Clin Orthop Relat Res 213:34–40
68. Burr DB (2004) Anatomy and physiology of the mineralized tissues: role in the pathogenesis of osteoarthrosis. Osteoarthritis Cartil, Osteoarthr Res Soc 12(Suppl A):S20–30
69. Buck RJ, Wirth W, Dreher D, Nevitt M, Eckstein F (2013) Frequency and spatial distribution of cartilage thickness change in knee osteoarthritis and its relation to clinical and radiographic covariates - data from the osteoarthritis initiative. Osteoarthritis Cartil, Osteoarthr Res Soc 21(1):102–109
70. Esmonde-White KA, Esmonde-White FW, Morris MD, Roessler BJ (2011) Fiber-optic Raman spectroscopy of joint tissues. Analyst 136(8):1675–1685